On the effect of fines content on the onset of internal instability and suffusion of sand mixtures

Author 1:

- Jitrakon Prasomsri
- PhD Candidate, Department of Civil and Environmental Engineering, Tokyo Institute of Technology, Tokyo, Japan
- ORCID: 0000-0001-9455-2655
- Email: jitrakon.mx@gmail.com

Author 2:

- Thomas Shire
- PhD, Lecturer in Geotechnical Engineering, James Watt School of Engineering, University of Glasgow, UK
- ORCID: 0000-0002-8005-5057
- Email: Thomas.shire@glasgow.ac.uk

Author 3:

- Akihiro Takahashi
- Professor, Department of Civil and Environmental Engineering, Tokyo Institute of Technology, Tokyo, Japan
- ORCID: 0000-0003-1206-5066
- E-mail: takahashi.a.al@m.titech.ac.jp

Corresponding author:

Akihiro Takahashi, Department of Civil and Environmental Engineering, Tokyo Institute of Technology, 2-12-1-M1-3 Oh-okayama, Meguro, Tokyo, Japan, 152-8552. Tel +81-3-5734-2593; Fax +81-3-5734-3577. E-mail: takahashi.a.al@m.titech.ac.jp

Géotechnique Letters 11, 2021.

Original URL:

https://dx.doi.org/10.1680/jgele.20.00089

Abstract

Internal instability or suffusion is one of the mechanisms of internal erosion in cohesionless soils, which is described by the loss of integrity of soil by seepage flow and is associated with the migration of finer particles. The contribution of the non-plastic finer fraction in a material is a key factor governing internal instability susceptibility. This study presents the experimental investigation of the influence of the fines content on the onset of internal instability of gap-graded sands using a pressure-controlled triaxial erosion device. The results indicate that the finer fraction in the soil has a significant influence on the hydraulic gradient at the onset of erosion. The underfilled soil with fines content less than 30% is vulnerable to suffusion at a relatively small hydraulic gradient. The transitional soil, whose fines content is between 30% and 35%, also exhibits suffusion, but the erosion onset hydraulic gradient significantly increases with increasing fines content. The overfilled soil with fines content larger than 35% exhibits suffosion or internal stability at a larger hydraulic gradient. The results also highlight the necessity of the multiple indices, such as mass loss, volumetric change and change in permeability, in evaluating the onset of various instability phenomena.

Keywords: Internal erosion; Suffusion; Seepage; Fabric/structure of soils

Notation

D_r	Initial relative density
D_{rc}	Relative density after consolidation
e_c	Global void ratio at the end of consolidation
e_{max}	Maximum void ratio
e_{min}	Minimum void ratio
e_s	Intergranular void ratio
$e_{s,max}$	Maximum void ratio of coarse particle
FC	Initial fines content (finer fraction)
FC^*	Transitional fines content (finer fraction)
FC_{max}	Maximum limit fines content (finer fraction)
i	Hydraulic gradient
i_e	Hydraulic gradient initiates erosion
k	Permeability
k_i	Initial permeability
k_e	End-of-test permeability
m_e	Eroded soil mass
p'_c	Mean effective stress at the end of consolidation
v	Seepage velocity
ε_v	Volumetric strain

Introduction

Internal instability describes the loss of integrity of soil by seepage flow and is associated with the migration of non-plastic finer particles in broadly and gap-graded soils. Instability has been divided into two phenomena depending on the occurrence of volume change: suffusion and suffosion (Fannin & Slangen 2014; USBR-USACE, 2015). The contribution of fines in the soil stress matrix could influence instability susceptibility as demonstrated by discrete element modelling (DEM) (Shire *et al.*, 2014; 2016). Depending on the fines content, they categorised the contribution of fines in the gap-graded soil into three conditions; underfilled, transition, and overfilled. The finer fraction in an underfilled soil is unstressed and could be eroded by suffusion. For overfilled soil, the finer fraction mainly contributes to the stress transmitting matrix; it could be eroded in the mode of either suffosion or fluidisation. Transition is complex and influenced by fines content, relative density, and gap-ratio. Limited experimental data that systematically examine fines content effects on suffusion, though complementary data exist for shear strength (Vallejo, 2001) and debris flows (Cui *et al.*, 2017). This paper aims to quantify the influence of fines on the onset of the instability of the gap-graded sands under the wide range of fines content. The gap-ratio and relative density are held constant to isolate the influence of fines content. The experimental findings provide an insight into the distinction of various instability phenomena depending on fines content.

Tested material, apparatus and testing programme

The gap-graded mixtures of Silica No. 3 as coarse fraction and Silica No. 8 as erodible finer fraction are used. When studying internal stability finer fraction refers to the fraction which can be eroded, so it should be noted that Silica No. 8 is regarded as a non-plastic finer fraction in this study, although its particle size is larger than that of fines by definition (i.e. silt and clay sized material). Silica No. 3 alone and seven mixtures with FC = 15, 20, 25, 30, 32.5, 35, and 40% (by mass) are tested in this study. Note that the FC by mass in this study is the same as that by volume since the specific gravity of all the particles is the same. Silicas No. 3 and No. 8 are categorized as sub-angular and angular, respectively (e.g., Altuhafi *et al.*, 2013). The properties of the Silicas and mixtures are summarized in **Table 1.** Their

gradations are presented in **Fig. 1**. For gap-graded specimens, D_{c15}/D_{f85} = 6.6, i.e., specimens are internally unstable to the Kézdi geometric criterion (Kézdi, 1979).

The triaxial erosion apparatus developed initially by Ke & Takahashi (2014), is modified and used to conduct the tests as depicted in a schematic diagram in **Fig. 2**. The modification is the capability of internal erosion experiments with a high back-pressure under a pressure-controlled condition. The chamber accommodates the cylinder specimens with 150 mm in height and 75 mm in diameter. The seepage flow is imposed downwardly from the inlet tank to the specimen by increasing the inlet tank pressure (*ITP*), while the base pressure (*BP*) of the specimen is maintained constant. The top pressure (*TP*) of the specimen is variable and measures actual head change. The hydraulic gradient (i) is determined by the differential pressure between *TP* and *BP* to the specimen length. The flow rate is measured at the top and is used to calculate seepage velocity (v). With this system, both seepage velocity and hydraulic gradient change during erosion testing. The data acquisition system records the pore pressures, flow rate, axial, radial displacements, and cumulative eroded soil mass. The volumetric strain (ε_v) is determined using axial and average radial displacements based on the right cylinder assumption with an accuracy of +/– 0.06%.

The specimens are reconstituted using the moist tamping method with 10% water content targeting D_r of 50%, according to Ladd (1978) and Jiang *et al*. (2003). The specimens are fully saturated with a back-pressure of 400 kPa and consolidated to p'_c = 50 kPa. The seepage flow is applied through the specimen by raising the *ITP* from 400 to 430 kPa with a rate of 2 kPa/min. The *BP* of 400 kPa and the zero-deviator stress are kept constant throughout the test. The test is terminated when the *ITP* reaches 430 kPa.

In this study, the mixture fabric is identified by plotting e_c – FC of each mixture on the fabric classification diagram shown in **Fig. 3**. In the figure, the lines corresponding to e_{min} and e_{max} determined according to Lade *et al.* (1998) are plotted along with the critical limits FC^* (= 30%) determined

according to Yang *et al.* (2006) and FC_{max} (= 35%) proposed by Skempton & Brogan (1994). At FC = FC*, the void formed by the coarser particles is filled with the finer fraction, and e_{max} and e_{min} show minimum values. Skempton & Brogan (1994) proposed that, if FC exceeds FC_{max}, the coarser particles float in a finer matrix, which was validated by DEM (Shire *et al.*, 2014). The zone bracketed by these indices is considered a transition zone. Accordingly, when FC < 30%, the soil has an "underfilled" fabric; the coarser particles are in contact that plays a primary role in soil skeleton, while the finer fraction offers a minor contribution. When 30% ≤ FC < 35%, the fabric is in transition; the contribution of finer particles to the soil stress matrix will be active, semi-active, or inactive. FC ≥ 35% gives an "overfilled" fabric; the coarser particles are floating within the finer matrix such that, the coarser particles are not in contact.

Test results and analysis

The test results are summarized in **Table 2**. The seepage response can be divided into two stages before and after the onset of erosion. Before the onset of erosion, the initial permeability (k_i) value, which is the slope of i – v curve, is approximately constant, with no change in m_e and ε_v (**Figs. 4** and **5**). The variation of ε_v in this stage is negligible since the magnitude is smaller than the measurement accuracy (+/– 0.06%).

At the onset of erosion, the finer particles start to erode from the specimen when the hydraulic gradient is larger than a certain value. Afterwards, the v, k, and ε_v start to change against i depending on FC and fabric type. The hydraulic gradient at the first detection of m_e is defined as the erosion onset hydraulic gradient (i_e), as indicated by a star symbol in **Fig. 4**.

The test on Specimen F0 is firstly conducted to be a companion specimen for potentially unstable specimens. k is essentially unchanged with absence in ε_v throughout the test (**Fig. 4**). This suggests that there is no change in fabric and the specimen is internally stable.

Specimens F15, F20, and F25 have underfilled fabric. For Specimens F15 and F20, the k progressively decreases with i when $i > 0.15$ and 0.51, respectively (**Fig. 4**). Meanwhile, the finer fraction starts to erode without a change in ε_v (**Fig. 5**). Accordingly, it could be judged that the finer fraction carries only minimum effective stress and erosion initiates at $i_e = 0.15$ and 0.51 for Specimens F15 and F20, respectively. This result agrees with Slangen & Fannin (2017) finding for sub-angular sand with similar gap-ratio and FC of 20% in upward flow test. The response was attributed to the presence of non-load-bearing finer particles. The decrease in permeability suggests that some detached particles may have caused clogging of pore throat within the specimen. This is likely due to the polydisperse nature of void constriction sizes, which DEM and experimental analyses have shown depends on the particle size distribution, relative density and particle shape (Wu *et al.*, 2012; Sjah & Vincens, 2013; Shire & O'Sullivan, 2016), meaning the finer fraction can be transported some way through a specimen before eventually clogging pores (Mehdizadeh *et al.*, 2020).

For Specimen F25, k firstly decreases and subsequently increases with i when $i > 0.86$ (**Fig. 4**). Meanwhile, an increasing m_e associated with a negligible ε_v is observed (**Fig. 5**), suggesting that the i_e is 0.86 and again the finer fraction carries only minimum effective stress for this specimen. The temporary decrease in k with i is attributed to the filtration of the detached finer particles, leading to partial clogging. As seepage velocity increases it can unclog these particles, leading to the subsequent increasing k observed in this case. A similar change in permeability was also observed by Rochim *et al.* (2017) and Zhong *et al.* (2018), indicating the combination of detachment, transport, and filtration of finer particles during the seepage-induced erosion. As clogging leads to a reduction in permeability, this could in turn lead to an increase in pore water pressure and an eventual blowout of fines (Sail *et al.*, 2011), which would then allow permeability to increase again.

Partial clogging relates to the formation of metastable clogging structures, the stability of which depends on the ratio of the pore constriction diameter to the fine diameter. Grain-scale experimental work has shown that larger constriction to fine ratios creates more unstable clogging structures such as

146 bridges which could be destabilised by vibration or a change in seepage velocity (Valdes &
147 Santamarina, 2008). More angular and elongated particles also lead to metastable clogging structures
148 at larger constriction to fine ratios (Valdes & Santamarina, 2008). The mechanics of clogging is
149 complex and can be investigated using coupled computational fluid dynamics and discrete element
150 method (CFD-DEM) (Remond, 2010). The seepage response in these specimens is deemed suffusion,
151 as initial constant permeability followed by mass loss accompanied by permeability change without a
152 marked volumetric strain.
153
154 Specimens F30 and F32.5 are in the transition. For Specimen F30, a much higher erosion onset gradient
155 is observed than for $FC \leq 25\%$. k slightly increases with i when $i > 6.77$ (**Fig. 4**). For Specimen F32.5,
156 a sudden increase in k with a drop in i is observed when $i > 11.58$ (**Fig. 4**). The increase in m_e without a
157 marked change in ε_v is observed in these specimens (**Fig. 5**). The i_e are 6.77 and 11.58 for Specimens
158 F30 and F32.5, respectively. Although i_e is significantly higher, the volumetric response is similar to
159 that in the underfilled specimens: suffusion. The drop in the hydraulic gradient immediately after the
160 onset of erosion in Specimen F32.5 is attributed to a localised preferential flow path induced by
161 suffusion.
162
163 Specimen F35 is an overfilled soil. A sharp increase in k with a drop in i is observed when $i > 13.18$
164 (**Fig. 4**). Meanwhile, a marked increase in m_e with a noticeable change in ε_v is observed (**Fig. 5**),
165 indicating the rearrangement of the coarse particles. ε_v is considered as its magnitude is greater than the
166 measurement accuracy. Because of the sudden loss of the finer fraction, the system cannot maintain the
167 water pressure at the specimen top, leading to the drop in the hydraulic gradient as shown in **Fig. 5**. It
168 is believed that as the coarser particles sit in the finer matrix, the departure of the finer fraction would
169 create a preferential pore throat among the coarser particles along with the specimen, leading to volume
170 contraction. The response is deemed suffosion, as initial constant permeability is followed by the
171 subsequent increase in permeability with the contractive volume change, which initiates that $i_e = 13.18$.
172 Specimen F40 is also an overfilled soil, which is beyond the limit of $FC = 35\%$. The k is relatively

unchanged throughout the test (**Fig. 4**). However, a marked increase in m_e corresponding to change in ε_v is observed when $i > 17.96$ (**Fig. 5**). In this case, the radial deformation of the specimen only around the bottom of the specimen is observed, indicating that the finer fraction erodes only near the bottom of the specimen. It could be judged that erosion initiates at $i_e = 17.96$, but the response is deemed internal stability.

Influence of fines content on initial condition and onset of instability

k_i represents the initial condition of the soils. **Figure 6** shows k_i plotted against FC and e_s along with $e_s = e_{s,max}$ line. If $e_s < e_{s,max}$, the coarse particles are in contact with one another (Salgado *et al.*, 2000), forming the interconnected pores and flow paths (Beven & Germann 1982). It is worth noting that k_i remains constant at $FC = 0 – 15\%$; for larger FC, k_i decreases with FC. This tendency is in agreement with Bandini *et al.* (2009), and Gomez *et al.* (2014). When $FC \leq 15\%$, $e_s < e_{s,max}$, water could flow freely through the pores and flow paths. When $FC > 15\%$, $e_s > e_{s,max}$, the finer fraction would fill in the pores; the flow paths would be obstructed by the finer fraction, leading to the decrease in permeability.

Figure 7 plots i_e and ε_v against FC with images showing the possible soil fabric. When $FC \leq 25\%$, the i_e and ε_v are close to zero. In the transitional zone, the i_e increase rapidly with FC with negligible ε_v. When $FC \geq 35\%$, both i_e and ε_v increase with FC. The significant changes in i_e and ε_v with FC are likely due to the contribution of finer fraction in the fabric and stress transfer (Shire *et al.*, 2014; 2016). For the underfilled soils, $FC < 30\%$, the coarse particles create a continuous matrix and form the constrictions, leaving finer fraction to float within the constrictions, likely as effective stresses are carried mainly by the coarse particles. Looking at $e_s > e_{s,max}$ for $FC = 20\%$ and 25%, this suggests that some finer particles are separating coarser particles sufficiently that the coarser fabric is altered. Either finer particles are lodged between coarser particles, or some voids are full of finer particles; this is heterogeneous. The lodged finer particles would be under high stress so will not be part of the erodible fraction. The unstressed finer particles are eroded by suffusion at a relatively small hydraulic gradient

without altering the coarse skeleton, but it would have a situation where a proportion of the finer fraction cannot be eroded.

In transition, 30% ≤ *FC* < 35%, it is believed that both coarser and finer fractions contribute to the soil matrix and the amount of finer fraction is sufficient for contact to be made among the particles and for the particles to be packed tightly in the voids formed by the coarse particles (Prasomsri & Takahashi, 2020). As the finer fraction is under stress, and coarser particles are in contact (on average), the finer fraction can be eroded by suffusion but require a relatively large hydraulic gradient. In this zone, the relative density would affect soil packing (Shire *et al.*, 2014), which needs further investigation.

For the overfilled soils with *FC* ≥ 35%, the coarser particles sit within the finer matrix and are not in contact. Most of the finer fraction is under stress and well-connected in the force chain network. The portion of the finer fraction can be eroded by suffosion at a larger hydraulic gradient, and their departure will cause readjustment of the soil fabric, resulting in a volume change.

Conclusions

The contribution of a non-plastic finer fraction in soil fabric is an important factor governing the onset of instability. The experimental results show that the underfilled soil with *FC* < 30% is vulnerable to suffusion (erosion of finer fraction without volumetric strain) at a relatively small hydraulic gradient. The transitional soil with 30% ≤ *FC* < 35% also shows suffusion, but at a larger hydraulic gradient. The overfilled soil with *FC* ≥ 35% exhibits suffosion (erosion of finer fraction with volumetric strain) or internal stability at a larger hydraulic gradient. For practical purposes, the fines content < 30% may be used as a discrimination point to recognise a concerning suffusion phenomenon. In this condition, the finer fraction can be eroded at a small hydraulic gradient without altering soil structure, which yields a change in permeability and may shift the soil to a looser state as a consequence of mass loss. However, the effect of gap ratio, relative density, and confining stress must also be taken into consideration.

During the erosion process, the mass loss, volumetric change, and change in permeability occur simultaneously and are fully combined. These multiple indices are necessary to evaluate the onset of instability.

Acknowledgements

The first author would like to acknowledge the scholarship support of the Japanese Government (Monbukagakusho: MEXT). This work was partially supported by JSPS KAKENHI Grant No. 19H02232.

References

Altuhafi, F., O'sullivan, C., & Cavarretta, I. (2013). Analysis of an image-based method to quantify the size and shape of sand particles. *J. Geotech. Geoenviron. Engng.* **139**, No. 8, 1290-1307.

Bandini, P., & Sathiskumar, S. (2009). Effects of silt content and void ratio on the saturated hydraulic conductivity and compressibility of sand-silt mixtures. *J. Geotech. Geoenviron. Engng.* **135**, No. 12, 1976-1980.

Beven, K., & Germann, P. (1982). Macropores and water flow in soils. *Water Resour. Res.* **18**, No. 5, 1311–1325.

Cui, Y. F., Zhou, X. J., & Guo, C. X. (2017). Experimental study on the moving characteristics of fine grains in wide grading unconsolidated soil under heavy rainfall. *Journal of Mountain Science*. **14** No. 3, 417–431.

Fannin, R. J., & Slangen, P. (2014). On the distinct phenomena of suffusion and suffosion. *Géotechnique Lett.* **4**, No. 4, 289–294.

Gomez, B. W., Dewoolkar, M. M., Lens, J. E., & Benda, C. C. (2014). Effects of fines content on hydraulic conductivity and shear strength of granular structural backfill. *Transp. Res. Rec.* **2462**, No. 1, 1–6.

Jiang, M. J., Konrad, J. M., & Leroueil, S. (2003). An efficient technique for generating homogeneous specimens for DEM studies. *Comput. Geotech.* **30**, No. 7, 579–597.

253 Ke, L., & Takahashi, A. (2014). Triaxial erosion test for evaluation of mechanical consequences of
254 internal erosion. *Geotech. Testing J.* **37**, No. 2.
255 Kézdi, A. (1979). *Soil Physics: Selected Topics*. Elsevier Scientific Publishing Co., Amsterdam.
256 Ladd, R. S. (1978). Preparing test specimens using undercompaction. *Geotech. Test. J.* **1**, No. 1, 16–23.
257 Lade, P. V., Liggio, C. D., & Yamamuro, J. A. (1998). Effects of non-plastic fines on minimum and
258 maximum void ratios of sand. *Geotech. Testing J.* **21**, 336–347.
259 Mehdizadeh, A., Disfani, M. M., & Shire, T. (2020). Post-erosion mechanical response of internally
260 unstable soil of varying size and flow regime. *Can. Geotech. J.*
261 Prasomsri, J., & Takahashi, A. (2020). The role of fines on internal instability and its impact on
262 undrained mechanical response of gap-graded soils. *Soils Found.*
263 Remond, S. (2010). DEM simulation of small particles clogging in the packing of large
264 beads. *Physica A: Statistical Mechanics and its Applications*. **389**, No. 21, 4485–4496.
265 Rochim, A., Marot, D., Sibille, L., & Thao Le, V. (2017). Effects of hydraulic loading history on
266 suffusion susceptibility of cohesionless soils. *J. Geotech. Geoenviron. Engng.* **143**, No. 7,
267 04017025.
268 Sail, Y., Marot, D., Sibille, L., & Alexis, A. (2011). Suffusion tests on cohesionless granular matter:
269 experimental study. *European Journal of Environmental and Civil Engineering*. **15**, No. 5, 799-
270 817.
271 Salgado, R., Bandini, P., & Karim, A. (2000). Shear strength and stiffness of silty sand. *J. Geotech.*
272 *Geoenviron. Engng.* **126**, No. 5, 451–462.
273 Shire, T., & O'Sullivan, C. (2016). Constriction size distributions of granular filters: a numerical
274 study. *Géotechnique.* **66**, No. 10, 826–839.
275 Shire, T., O'Sullivan, C., & Hanley, K. J. (2016). The influence of fines content and size-ratio on the
276 micro-scale properties of dense bimodal materials. *Granul. Matter.* **18**, No. 3, 52.
277 Shire, T., O'Sullivan, C., Hanley, K. J., & Fannin, R. J. (2014). Fabric and effective stress distribution
278 in internally unstable soils. *J. Geotech. Geoenviron. Engng.* **140**, No. 12, 04014072.

279 Sjah, J., & Vincens, E. (2013). Determination of the constriction size distribution of granular filters by
280 filtration tests. *International Journal for Numerical and Analytical Methods in Geomechanics*. **37,**
281 No. 10, 1231-1246.
282 Skempton, A. W., & Brogan, J. M. (1994). Experiments on piping in sandy
283 gravels. *Géotechnique.* **44**, No. 3, 449–460.
284 Slangen, P., & Fannin, R. J. (2017). The role of particle type on suffusion and
285 suffosion. *Géotechnique Lett.* **7**, No. 1, 6–10.
286 USBR-USACE (US Bureau of Reclamation-US Army Corps of Engineers) (2015). *Best practices in*
287 *dam and levee safety risk analysis*, Technical Report Version 4.0. US Bureau of Reclamation and
288 the US Army Corps of Engineers, Denver, CO, USA.
289 Valdes, J. R., & Santamarina, J. C. (2008). Clogging: bridge formation and vibration-based
290 destabilization. *Can. Geotech. J.* **45**, No. 2, 177–184.
291 Vallejo, L. E. (2001). Interpretation of the limits in shear strength in binary granular mixtures. *Can.*
292 *Geotech. J.* **38**, No. 5, 1097–1104.
293 Wu, L., Nzouapet, B. N., Vincens, E., & Bernat-Minana, S. (2012). Laboratory experiments and the
294 determination of the constriction size distribution of granular filters. In *Proceedings of 6th*
295 *international conference on scour and erosion (ICSE-6)*, 233–240, Paris, France.
296 Yang, S., Lacasse, S., & Sandven, R. (2006). Determination of the transitional fines content of
297 mixtures of sand and non-plastic fines. *Geotech. Testing J.* **29**, No. 2, 102–107.
298 Zhong, C., Le, V. T., Bendahmane, F., Marot, D., & Yin, Z. Y. (2018). Investigation of spatial scale
299 effects on suffusion susceptibility. *J. Geotech. Geoenviron. Engng.* **144**, No. 9, 04018067.

List of captions for all tables

List of captions for all figures

Table 1 Physical and gradation properties of test materials

Physical and gradation properties	Silica sands		Mixtures (%)						
	No. 3	No. 8	15	20	25	30	32.5	35	40
Specific gravity, G_s	2.645	2.645	2.645	2.645	2.645	2.645	2.645	2.645	2.645
Maximum void ratio, e_{max}	0.98	1.24	0.79	0.76	0.73	0.70	0.70	0.72	0.73
Minimum void ratio, e_{min}	0.75	0.88	0.54	0.48	0.44	0.40	0.41	0.42	0.43
Uniformity coefficient, C_u	1.47	2.18	9.27	10.49	11.41	11.35	12.40	12.65	13.09
Curvature coefficient, C_c	1.60	0.98	4.30	5.09	5.35	1.98	0.45	0.38	0.31
D_{c15} (mm)	1.65	–	–	–	–	–	–	–	–
D_{f85} (mm)	–	0.25	–	–	–	–	–	–	–
Median aspect ratio, AR_{50}	0.73	0.65	–	–	–	–	–	–	–
Median convexity, Cx_{50}	0.95	0.92	–	–	–	–	–	–	–
Median sphericity, Sp_{50}	0.86	0.83	–	–	–	–	–	–	–
Particle description	Sub-angular ~ Angular								
Soil classification, *USCS*	Poorly graded sand (SP)								

Note: D_{c15} = D of 15% of F in coarser fraction; D_{f85} = D of 85% of F in finer fraction; D = particle diameter; F = mass passing by weight.

Table 2 Summary of major parameters in erosion tests

Test code	Initial conditions						Onset and end-of-test conditions				Fabric	Change in k after onset of erosion	Marked volumetric strain	Phenomenon
	FC (%)	e_c	e_s	D_{rc} (%)	B-value	k_i (cm/s)	i_e	m_e (g)	ε_v (%)	k_e (cm/s)				
F0	0	0.86	0.86	52	0.96	0.555	–	–	0.01	0.555	UF	↔	No	IS
F15	15	0.67	0.96	53	0.96	0.556	0.15	3.4	0.01	0.388	UF	↓	No	SU
F20	20	0.61	1.01	53	0.98	0.196	0.51	3.3	0.02	0.105	UF	↓	No	SU
F25	25	0.59	1.12	52	0.96	0.042	0.86	6.6	0.01	0.041	UF	↓↑	No	SU
F30	30	0.55	1.21	52	0.97	0.019	6.77	1.4	0.01	0.021	TF	↑	No	SU
F32.5	32.5	0.54	1.29	54	0.98	0.015	11.58	4.0	0.01	0.033	TF	↑	No	SU
F35	35	0.55	1.38	56	0.98	0.013	13.18	15.4	0.16	0.049	OF	↑	Yes	SO
F40	40	0.58	1.63	53	0.99	0.008	17.96	9.3	0.19	0.007	OF	↔	Yes	IS

Note: UF = underfilled fabric; TF = transitional fabric; OF = overfilled fabric; ↔ = constant; ↓ = decrease; ↑ = increase; IS = internal stability; SU = suffusion; SO = suffosion.

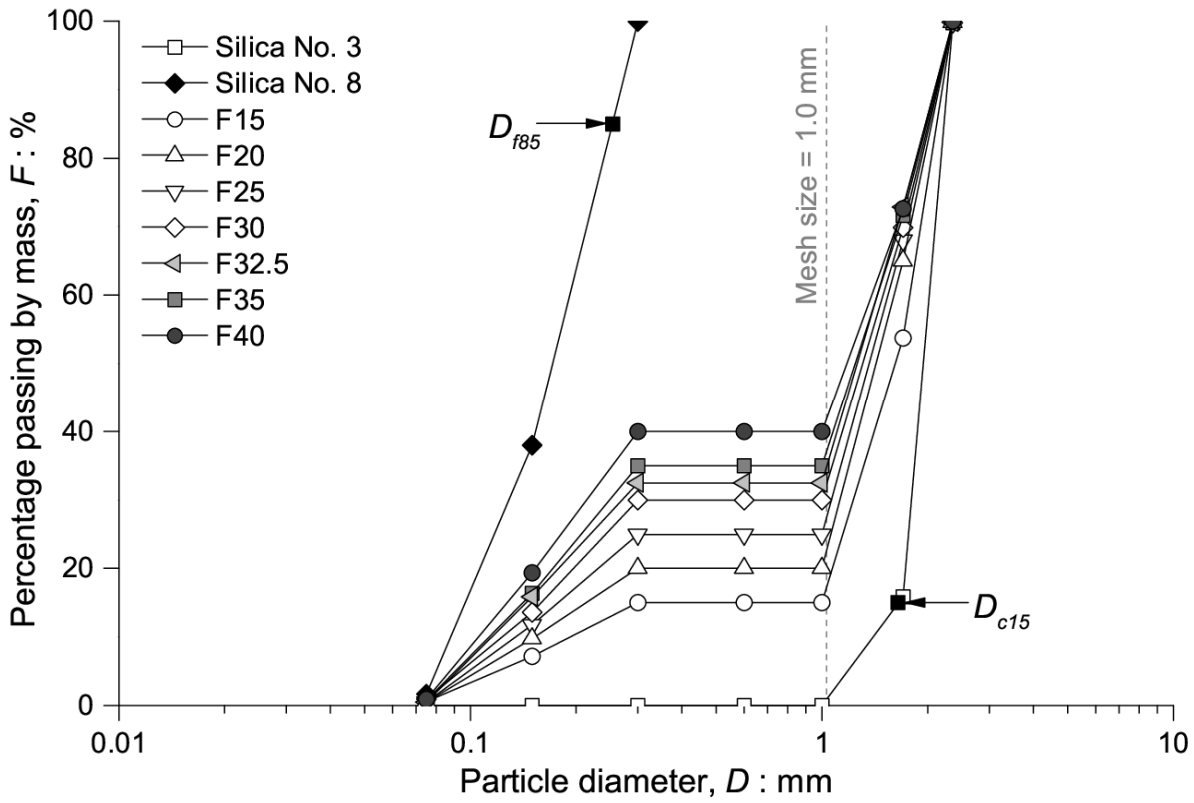

Fig. 1 Particle size distribution curves of the soils

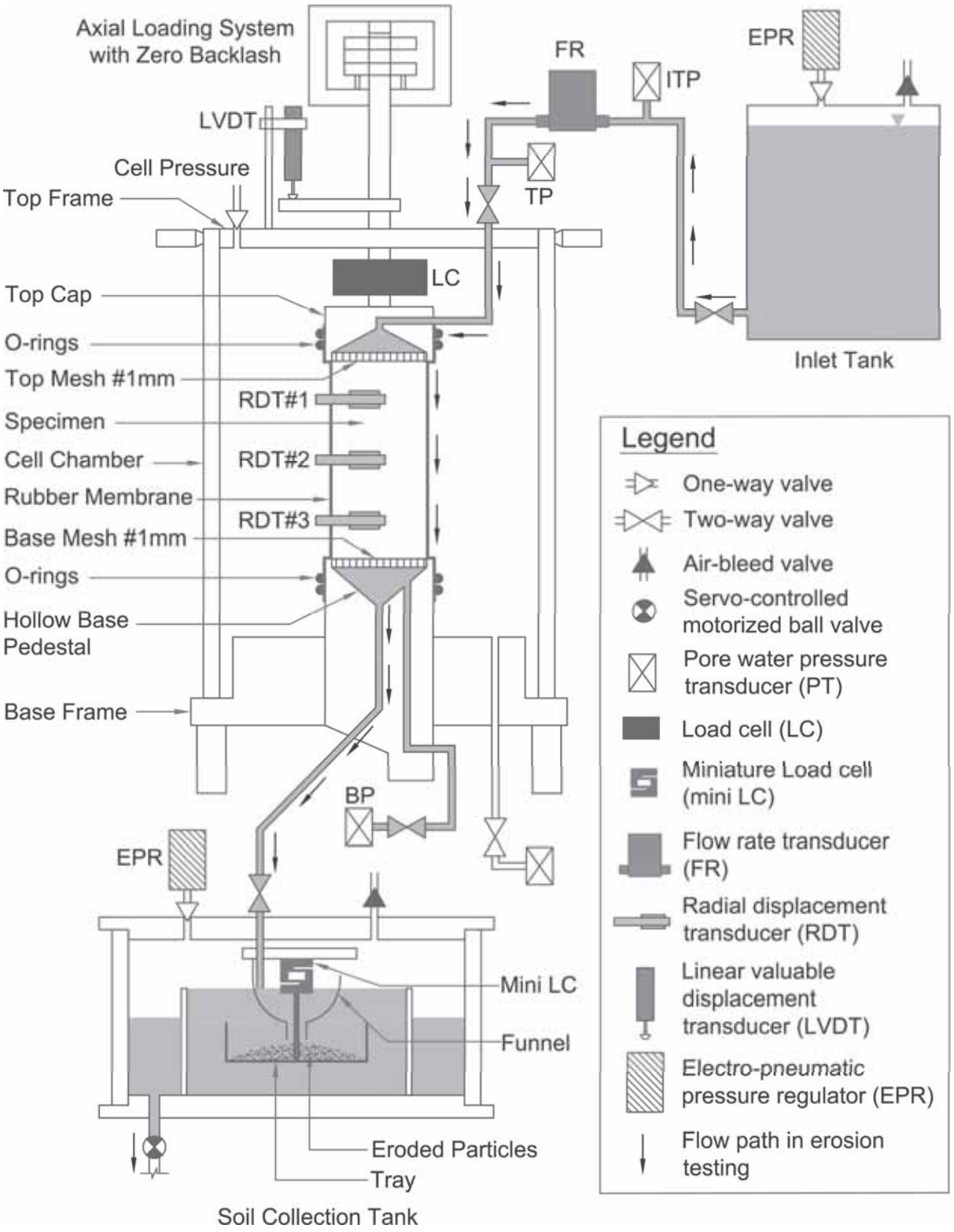

Fig. 2 General configuration of the pressure-controlled triaxial erosion apparatus

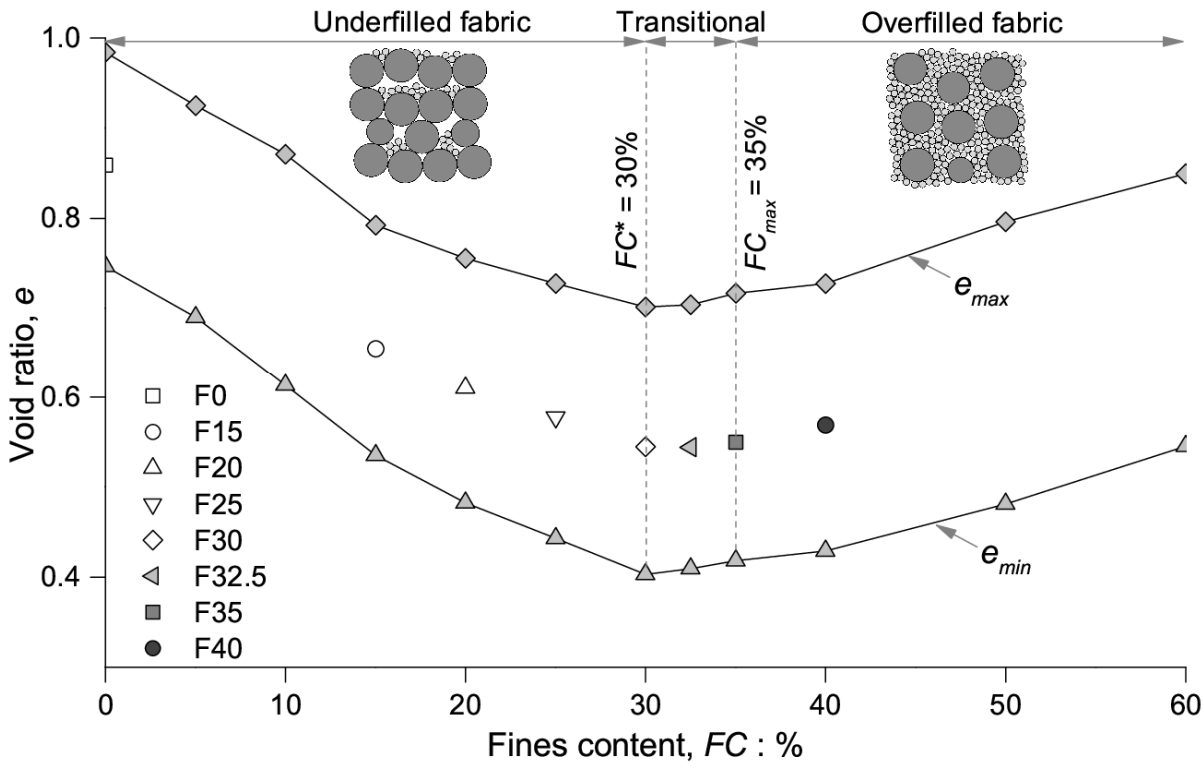

Fig. 3 Fabric classification diagram

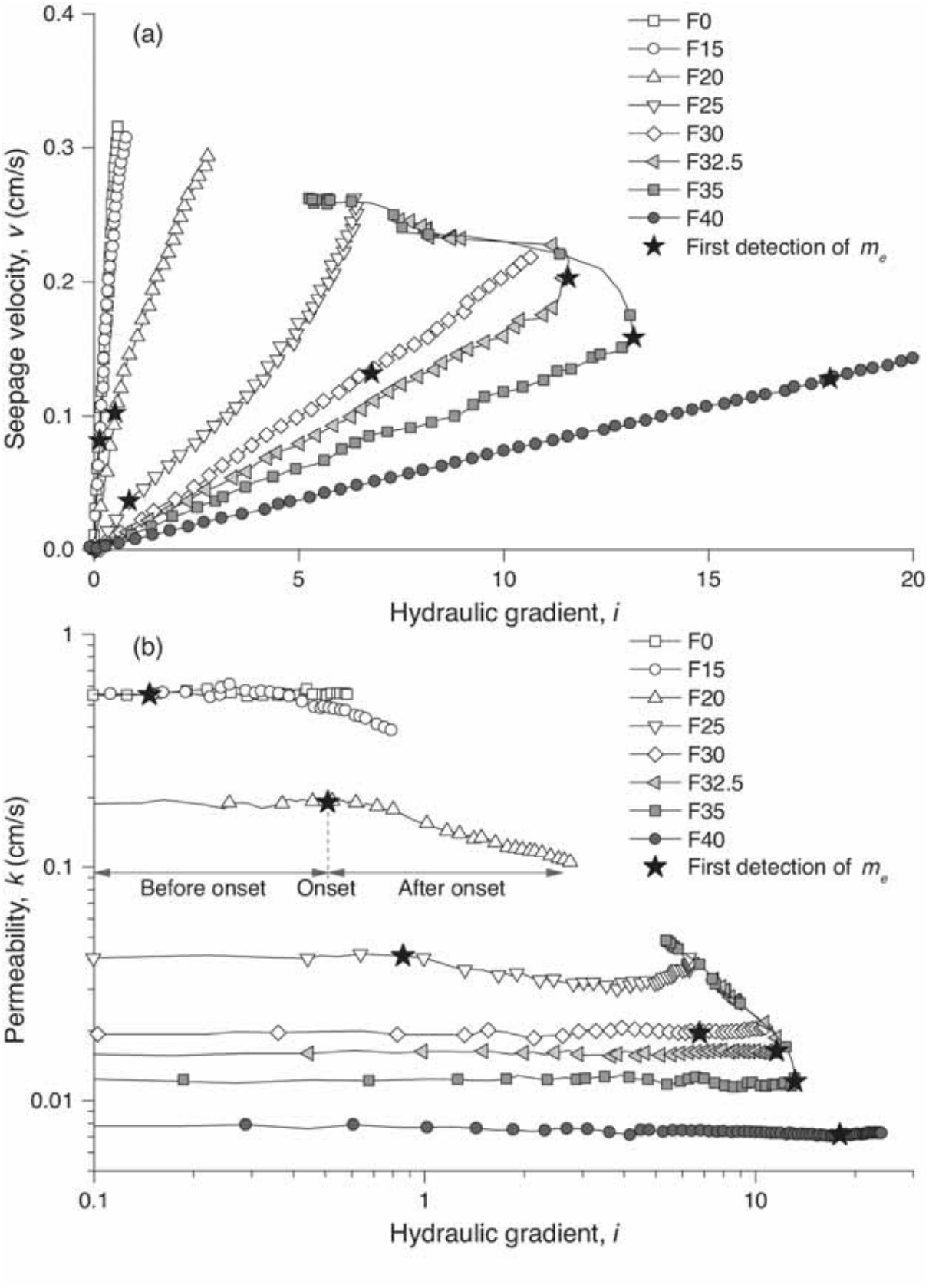

Fig. 4 Relationship between (a) seepage velocity, (b) permeability and hydraulic gradient

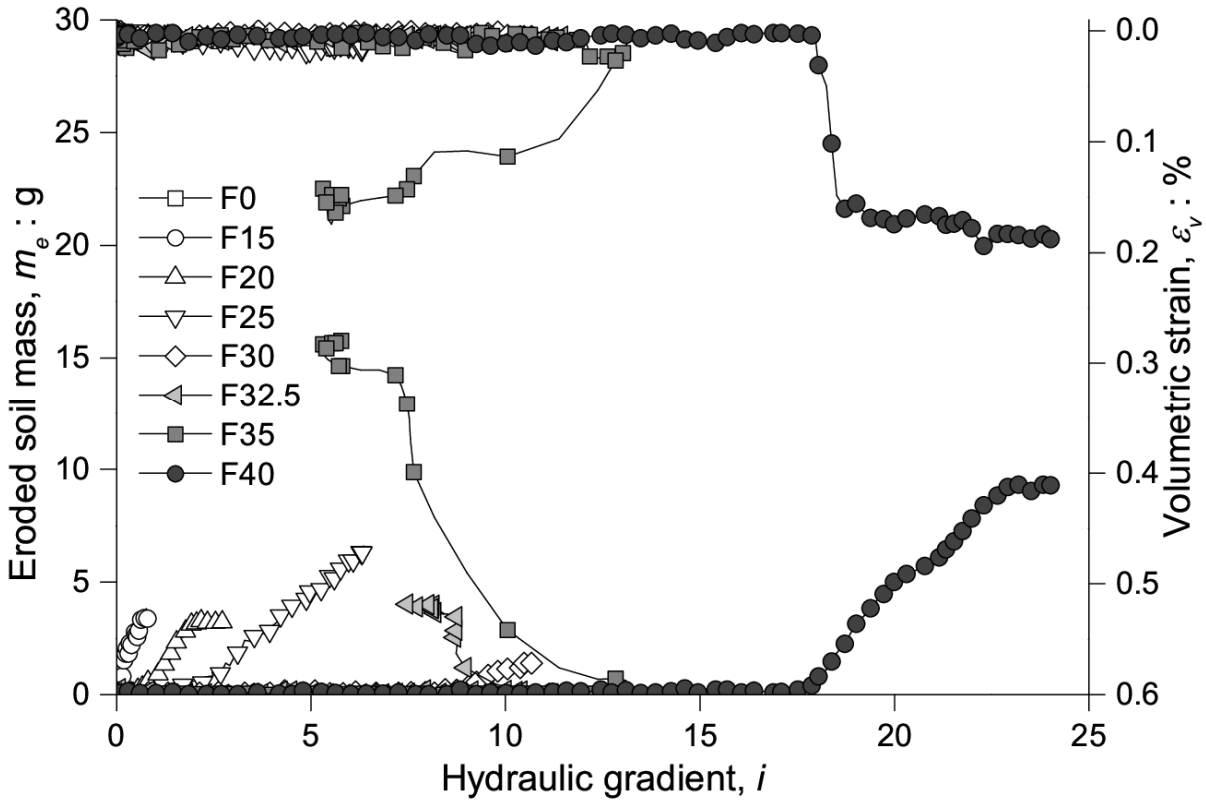

Fig. 5 Relationship between eroded soil mass, volumetric strain and hydraulic gradient

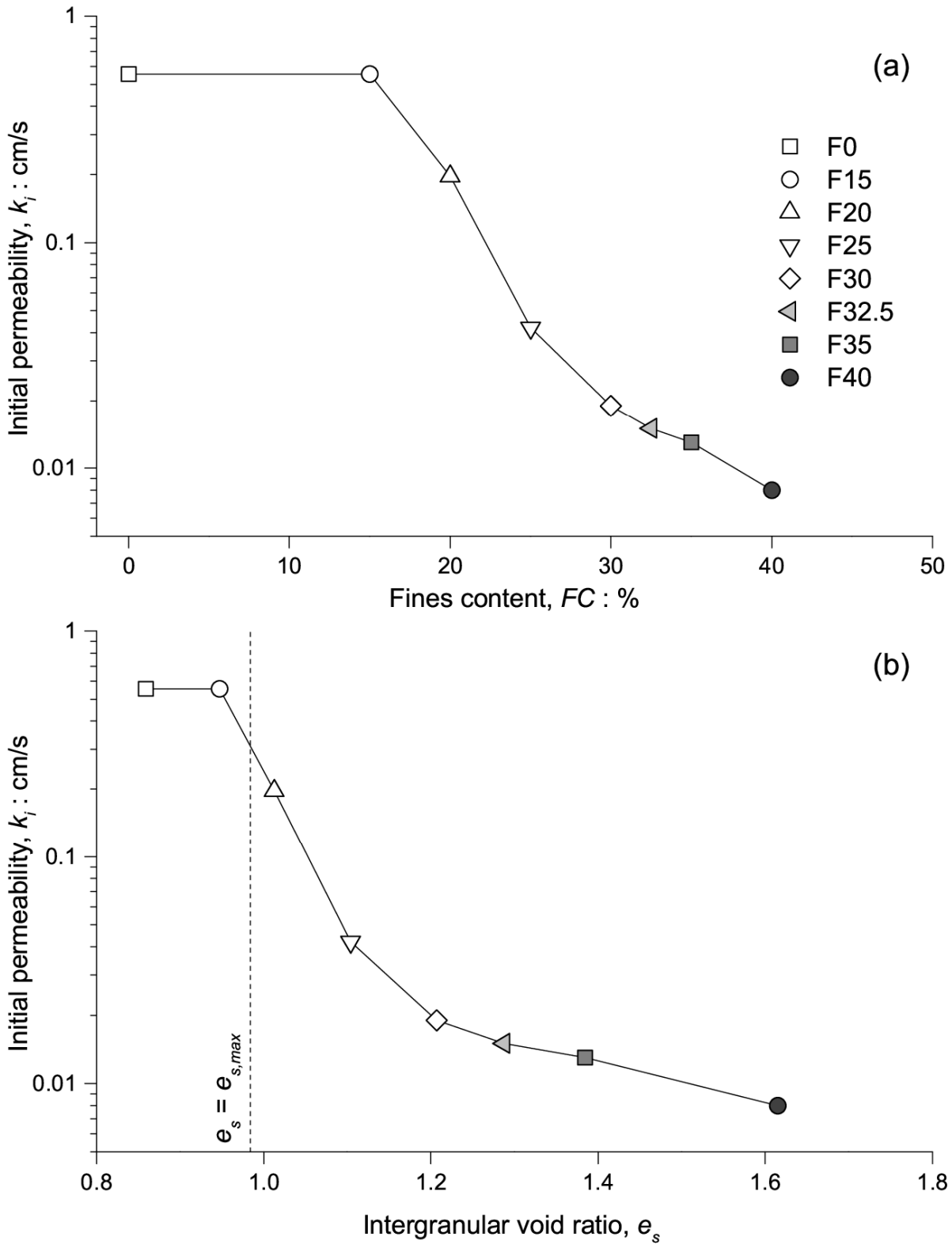

Fig. 6 Initial permeability against (a) initial fines content and (b) intergranular void ratio

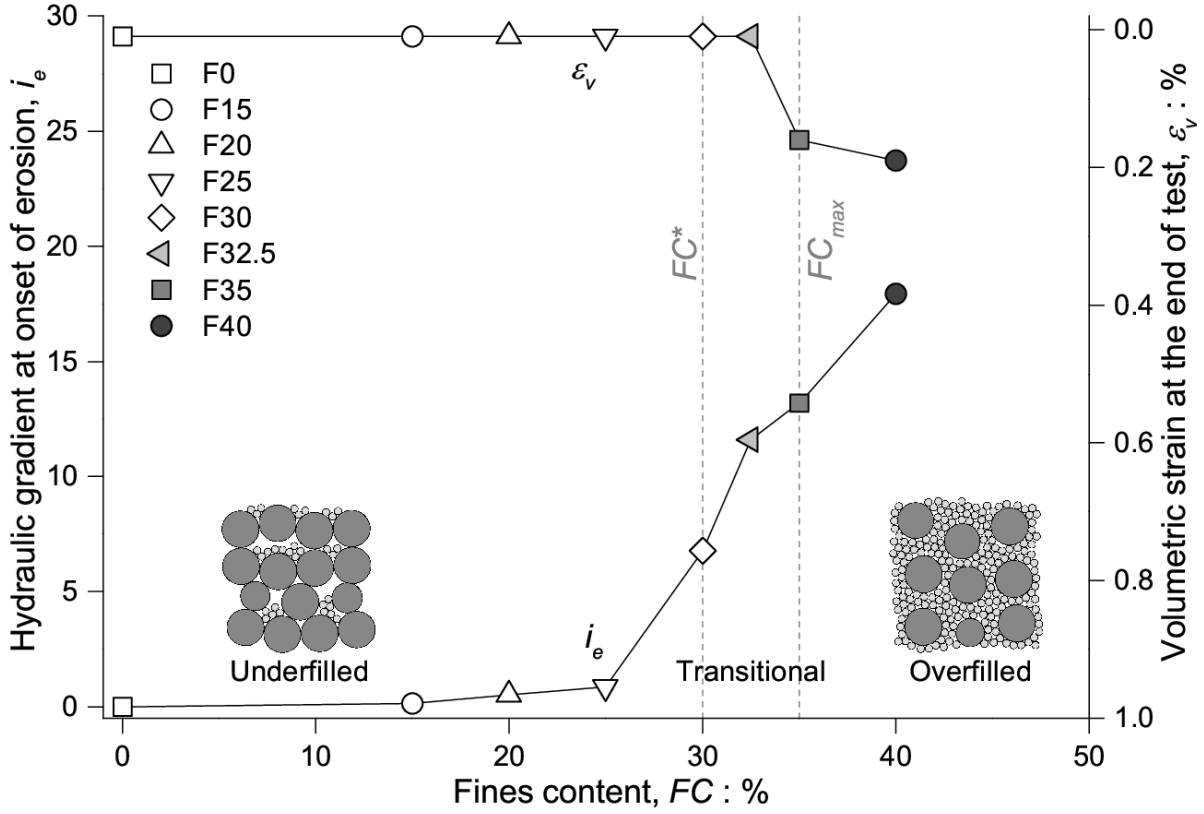

Fig. 7 Hydraulic gradient initiates erosion and volumetric strain at the end of test against initial fines content